Metal Foaming Studied *In-situ* by Energy Dispersive XRD of Synchrotron Radiation, X-ray Radioscopy, and Optical Imaging

C. Jiménez[1,2], F. Garcia-Moreno[1,2], B. Pfretzschner[1,2], P. Kamm[1,2], T. Neu[1,2], M. Klaus[2], Ch. Genzel[2], A. Hilger[2], I. Manke[2], J. Banhart[1,2]

[1] Materials Science and -Technology, Technical University Berlin (D-10623) Germany
[2] Institute of Applied Materials, Helmholtz Centre Berlin (D-14109) Germany

Abstract

To elucidate the phase transformations of TiH_2 inside liquid metal foams and their relationship with expansion, can provide deeper insight into metal foaming and help improve metal foam technologies. Therefore, we implemented three simultaneous *in-situ* methods based on synchrotron radiation that let follow: first, the phase transformations of TiH_2 inside AlSi11 precursors by energy dispersive XRD. Second, the foam structure was monitored by X-ray radioscopy, and third, a synchronized video camera recorded the foam expansion. TiH_2 particles transform differently inside expanding AlSi11 foams than the loose powder heated under inert gas flow due to reaction with the melt.

1   Introduction

The phase transformations of TiH_2 powder inside expanding foams and its relationship with expansion behaviour are still unknown aspects of metal foaming. TiH_2 is since many years the most commonly used blowing agent for making Al-based foams by either powder metallurgical or melting routes [1]. Different pre-treatments were optimized to shift the onset of H_2 release from the TiH_2 [2 − 6] towards higher temperatures inside the melting range of the most commonly used Al-based alloys, or pressing powder mixtures under vacuum, are examples of practices that lead to larger expansion and more regular pore size foaming at ambient pressure [7 − 9]. Reducing the melting temperature range by alloying Al with Si, Cu, Mg, Zn, or combinations of these elements are also successful strategies for producing foams of improved pore structure and properties [10 − 14]. However the more alloyed Al is the more complicated is to predict how the decomposition of TiH_2 will be inside expanding foams.

Recently the correlation between regimes of H_2 release and phase transformations of both as-received and pre-oxidised TiH_2 powders under flowing Ar were clarified, using a combination of in situ diffraction methods, thermoanalysis and electron microscopy that helped develop core shell models to describe the decomposition of TiH_2 in both conditions [15]. However, studies on H_2 desorption from foamable precursor material made for example by the powder metallurgical route [16], show different behaviour than the one from loose powders [17, 4, 9]. Therefore, experiments dedicated to study the decomposition of TiH_2 inside liquid metallic foams and its relation with expansion are needed and motivated the present work.

We combined three simultaneous in-situ methods to follow for the first time, the phase transformations of as-received and pre-oxidised TiH_2 inside expanding AlSi11 precursors
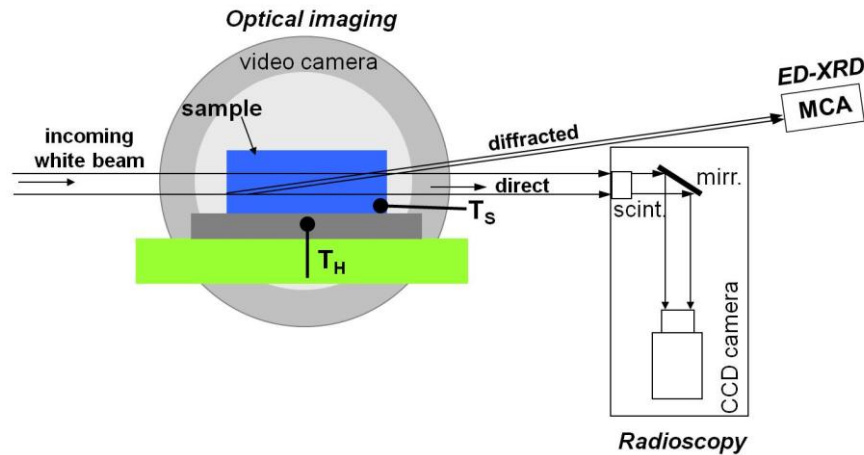
Figure 1. Setup used for studying in situ metal foaming. The incoming white beam is partially diffracted and used for following the phase transformations by ED-XRD. The directly transmitted part of the beam let monitor the foam structure and density. In addition, a synchronized video camera followed the overall foam expansion.

prepared by the powder metallurgical route at the EDDI experimental station of the synchrotron facility BESSY II in Berlin. We applied typical temperature profiles used for metal foaming and followed in situ the phase transformations by energy dispersive XRD and monitored details of the foam structure and foam density by X-ray radioscopy. A synchronized video camera recorded the overall foam expansion.

2   Materials and Methods

2.1   Foamable precursor material preparation

Silicon (Wacker Chemie GmbH, purity 99.5%), aluminium (Alpoco Ltd., purity 99.7%) and TiH_2 powder (Chemetall GmbH, purity 98.8 %, particle size < 36 μm) were used for this work. Part of the TiH_2 was pre-oxidised at 480 ℃ for 180 minutes in air. Then powders were blended to prepare the alloys AlSi11 + 5 wt.% of either as-received or pre-oxidised TiH_2. We prepared tablets of 30 g mass and 36 mm diameter by uni-axial hot-compaction applying 300 MPa under vacuum inside a chamber able to keep gas pressure below 8×10^{-2} mbar. A pre-compaction step was done at ambient temperature for 30 s and after heating at 10 K·min^{-1} up to 400 ℃, hot-compaction was performed for 300 s. The tablets were cut to foamable samples of $8 \times 8 \times 3$ mm^3 size. The 3 mm in height matches with the compaction direction.

2.2   Foaming followed by ED-XRD, optical imaging and X-ray radioscopy

Figure 1 shows a schematic side-view of the experimental setup used for studying in situ the foaming process at the EDDi experimental station hosted at the synchrotron facility BESSY II of the Helmholtz Centre Berlin.

A cavity was machined onto the sample in order to measure the sample temperature T_S with a thermocouple. The samples were placed on the heating plate of an Anton Paar DHS 1100 furnace and a second thermocouple measured the heater temperature T_H. Foaming was conducted in air, induced by increasing T_H from 30 to 700 ℃ at 100 K·min^{-1}. T_H was held

at 700 °C for 90 s and then cooling at -100 K·min^{-1} started. Additional foaming experiments also were performed at 700 °C but varying temperature at 40 K·min^{-1}.

For ED-XRD, the samples were illuminated with a white beam of X-rays of 3×1 mm^2 cross-section. The energy of diffracted photons was measured in transmission at a fixed position ($2\theta = 6°$) by a Ge multi-channel analysing detector that acquired one spectrum every 7.2 s. Further instrumental details of EDDi can be read in Ref 18.

For X-ray radioscopy, a fast PCO 1200 CCD camera (1280x1024 pixels) was used. The X-rays were converted into visible light by applying a LuAG scintillator screen with 200 µm thickness that is suited for the high thermal loads of the white X-ray beam. The light from the scintillator was reflected by 90° by a mirror onto a Nikon Nikkor lens (200 mm) that transfers the light onto the CCD chip. The mirror was necessary to prevent damage to the lens due to the extremely high intensity of the synchrotron X-ray beam. A 1:1 magnification was used, i.e. the pixel size in the radiographic images is identical to that of the CCD camera, i.e. 12x12 µm^2. Detector and lens were placed into a light-tight box. The achieved spatial resolution was about 30 µm. The exposure time was 15 ms and a delay time of 185 ms was used between the images. Thus 5 images per second were taken.

In addition, a synchronized video camera acquired 1 image per s to follow the overall foam expansion. Image radioscopic and optical sequences were analysed a posteriori with the free available software Image J.

2.3   Mass spectrometry

Complementarily, we studied hydrogen evolution from precursors containing as-received and pre-oxidised TiH$_2$ as function of time and temperature by mass spectrometry. For this we used a Netszch 409 C thermoanalyser which has a tubular furnace coupled via a skimmer to a quadrupole mass spectrometer. Samples, atmosphere and temperature profiles were the same as those used at EDDi (described in section 2.2).

3   Results and Discussion

3.1   Foaming AlSi11 with as-received TiH$_2$

The first example of foaming followed in situ at EDDi for AlSi11 containing 5 wt.% as-received TiH$_2$ is given in Figure 2. The area expansion of the precursor as function of time and temperature is calculated from the optical image sequence. Particular stages of expansion are visible in the images acquired at the times 6, 355, 405, 460 and 670 s. The radioscopic sequence shows the foam structure at the same times within a field of view of 2.5 × 0.8 mm^2 centred inside the X-ray beam cross-section. The sequence of radiograms reveals horizontal striations at 355 s corresponding to typical crack-like pores that appear in AlSi11 foams at early stages of expansion [9]. After 460 s the lighter parts of radiograph indicate the presence of bubbles but this foam is too dense to show the foam structure more clearly. The radiogram at 670 s shows the solid foam structure which is denser than at 460 due to shrinkage during cooling and implies that from this radiographic sequence one could extract the foam density evolution as well.

The map of diffracted intensities (colour scale) dispersed in energies obtained by ED-XRD contains the principal diffraction lines of each crystalline phase which evolve in time and temperature. For the applied heating rate 100 K·min^{-1}, the temperature resolution is 7 K. The

starting phases are Al, Si, and as-received TiH_2 whose respective diffraction lines move towards lower energies due to thermal expansion since diffracted photon energies are inversely proportional to plane-spacing ($E \propto d^{-1}$). At 533 °C the lines of TiH_2 move to higher energies, indicating that its lattice parameter starts shrinking due to the onset of H_2 release [15]. Inside this precursor heated at 100 K·min^{-1} the onset temperature 533 °C is shifted by 158 K to higher temperatures with respect to the 375 °C reported for the same event from loose powders heated at 10 K·min^{-1} under Ar flow [15].
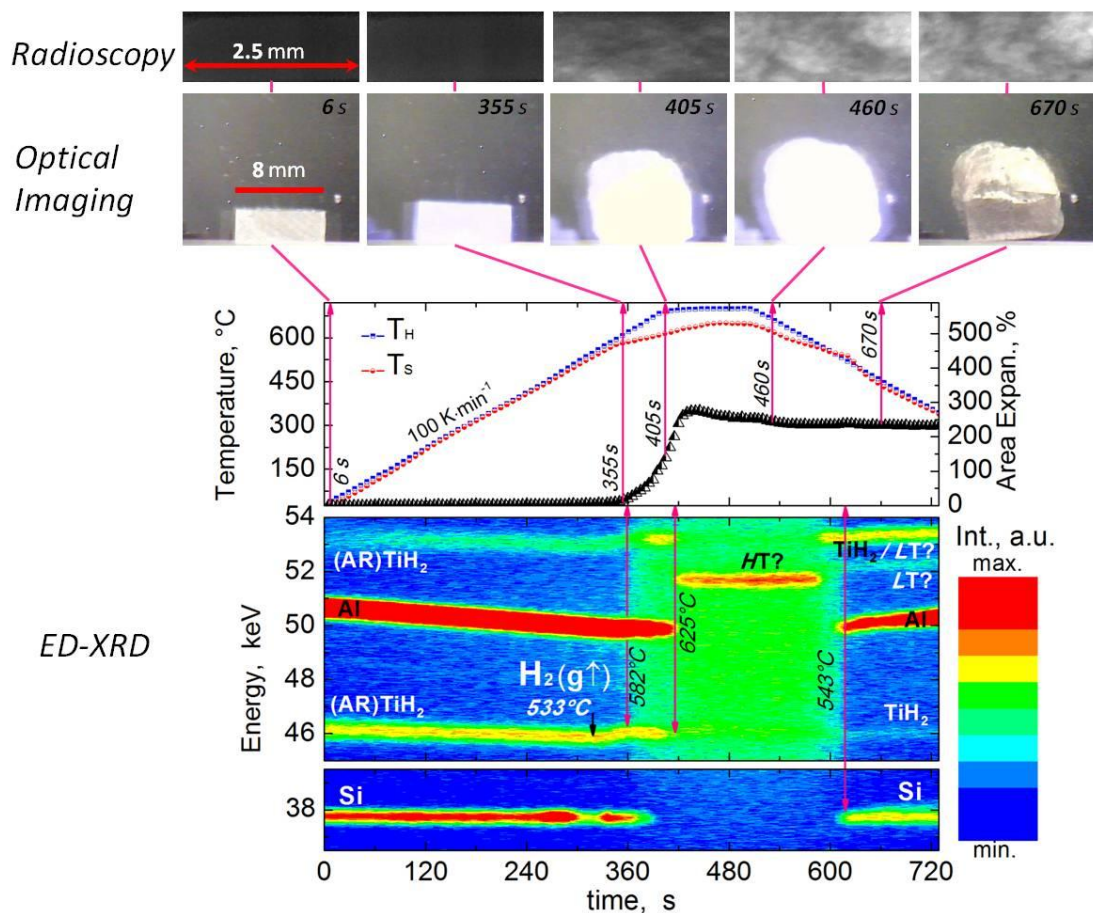
Figure 2. Synchronized radioscopic and optical image sequences synchronized with the map of diffracted intensities dispersed in energies as function of time that shows the phase transformations in AlSi11 + 5 wt.% as-received TiH_2 during foaming.

Melting starts during heating at 582 °C, fairly close to the eutectic temperature 577 °C, when the background increases due to the diffuse scattering coming from the liquid, and ends at 543 °C on cooling. The melting start is correlated with the onset of foam expansion and occurs close to the Si particles where the eutectic composition is easily achieved. When the Si line disappears, all the Si is dissolved in the melt and expansion rate of the foam increases. The diffraction line of Al disappears at 625 °C and a new high temperature phase appears labelled by *H*T. This phase is not clearly identified yet but is none of the hydrogen solid solutions of Ti β (bcc) or α (hcp) that appear during decomposition of TiH_2 loose powders under Ar flow [15]. According to the literature we should expect a Ti silicide belonging to the ternary system Al-Si-Ti but for a clearer identification, we need further in situ experiments with longer counting time than 7 s [19]. During cooling, *H*T transforms into another structure de-

nominated LT which is also not identified yet, but is not TiH_2 because the principal line of TiH_2 is close to 46 keV, whereas LT has its principal diffraction line close to 53.5 and a second line at lower energies. Some TiH_2 is retained after cooling as can be seen by its principal line close to 46 keV due to the fast heating and cooling rates. If heating and cooling rates are reduced to 40 K·min^{-1} this line no longer appears after cooling as can be seen in Figure 4 a.

3.2 Foaming AlSi11 with pre-oxidised TiH$_2$
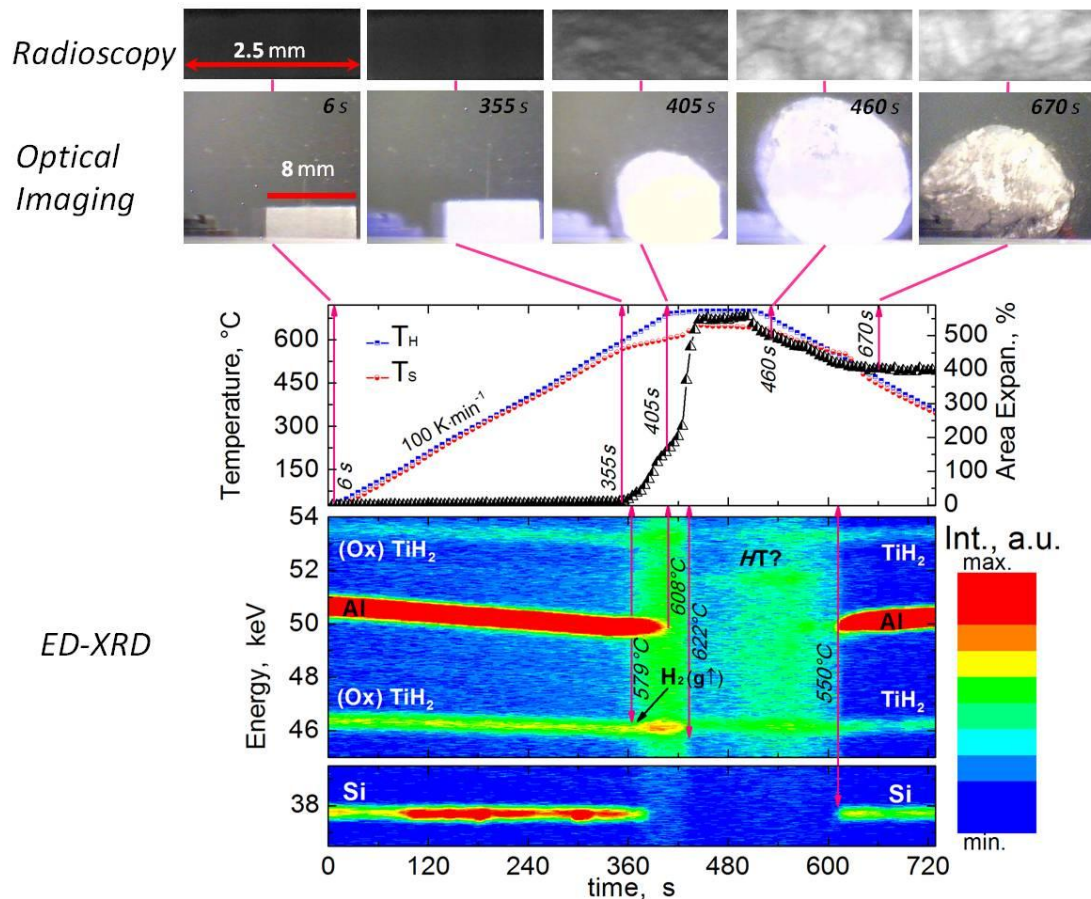
Figure 3. Same as in Figure 2 but for AlSi11 + 5 wt.% pre-oxidised TiH$_2$ during foaming.

Figure 3 is the analogous of Figure 2 but for AlSi11 foamed with 5 wt.% pre-oxidised TiH$_2$. The pre-oxidation shifts the onset of H$_2$ gas release form TiH$_2$ to 579 °C which is the temperature when melting starts. Expansion is also triggered by melting of the precursors and accelerates significantly from 622 °C, presumably due to the formation of HT. The pre-oxidation also stabilizes the hydride structure which remains during the whole foaming process, hindering the reaction with the liquid that results in the formation of the silicide HT and subsequently LT which is actually absent in this sample but starts to appear if the same material is heated at cooled at 40 K·min^{-1} (see Figure 4 b). This foam containing pre-oxidised TiH$_2$ reaches 550 % maximum and 400 % end expansions, whereas the foam made using as-received TiH$_2$ that reached 275 % and 240 % for the same values. The larger expansion let see more clearly in the radiogram at 460 s bubbles and cell-walls inside the liquid foam.

3.3 H₂ gas evolution

Additional maps of diffracted intensities obtained heating and cooling at 40 K·min⁻¹ are compared with characteristic curves of H₂ release followed by mass spectrometry in Figure 4.
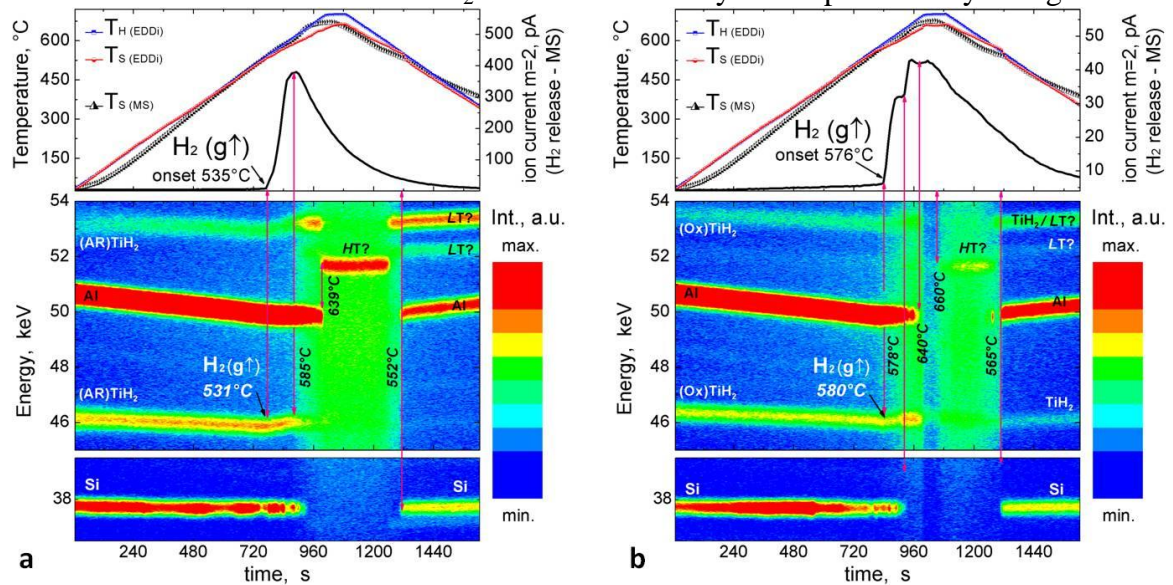
Figure 4. Phase transformation sequences compared to H₂ gas evolution for AlSi11 with 5 wt.% addition of a) as-received TiH₂ and b) pre-oxidised TiH₂.

The two complementary in situ techniques confirm that the H₂ gas released below melting from precursors made using as-received TiH₂ is totally lost since does not result in expansion of the precursor (See Figure 2). Only when melting starts, H₂ gas losses monotonically decrease. The pre-oxidation of TiH₂ reduces the losses by about one order of magnitude as can be noticed by comparing ion current scales in Figure 4 a and b.

4   Summary

The phase transformations of TiH₂ inside liquid metallic foams made by the powder metallurgical route were followed in situ by ED-XRD for the first time. Its relationship with expansion was studied by two synchronized imaging techniques. Optical imaging was used for calculating the foam expansion and X-ray radioscopy for following the evolution of the foam structure.

In this paper we show that the phase transformation sequences of TiH₂ during decomposition inside expanding AlSi11 foams differ from that observed for loose TiH₂ powders. We also found reasons for the positive effect of using pre-oxidised TiH₂ powder instead of as-received TiH₂ for foaming AlSi11 PM precursor material. The pre-oxidation of TiH₂ shifts the onset of H₂ release precisely up to the temperature when melting of the alloy starts. This reduces the H₂ gas loss by hindering the reaction of TiH₂ with the melt that accelerates its decomposition.

This combination of in situ methods provides a much deeper insight for studying the metal foaming process and can be extended to other alloys.

5   References

[1]   J. Banhart, Prog Mater Sci, 46, 559 (2001).

[2]   A. R. Kennedy, Scripta Mater 47, 763 (2002).

[3]   V. Gergely and B. Clyne, Adv. Eng. Mater, 2 , 175 (2000).

[4]   B. Matijasevic-Lux, J. Banhart, S. Fiechter, O. Görke, N. Wanderka, Acta Mater 54, 1887 (2006).

[5]   D. Lehmhus, G. Rausch, Adv Eng Mater 6, 313 (2004).

[6]   P. M. Proa-Flores and R. L. A. Drew, Adv Eng Mater 10, 830 (2008).

[7]   A. R. Kennedy, V. R. Lopez, Mater Sci Eng A 357, 258 (2003).

[8]   B. Matijasevic and J. Banhart, Scripta Mater, 54, 503 (2006).

[9]   C. Jiménez, F. Garcia-Moreno, M. Mukherjee, O. Goerke, J. Banhart, Scripta Mater 61, 552 (2009).

[10]   I. Duarte, J. Banhart, Acta Mater 48, 2349 (2000).

[11]   D. Lehmhus, M. Busse, Adv. Eng. Mater. 6, 391 (2004).

[12]   H.-M. Helwig, F. Garcia-Moreno, J. Banhart, J Mater Sci, 46, 5227 (2011).

[13]   M. Lafrance, M. Isac, F. Jalilian, K.E. Waters, R.A.L. Drew, Mater Sci and Eng A, 528, 6497 (2011).

[14]   K. Kitazono, Y. Takiguchi, Scripta Mater. 2006, 55, 501.

[15]   C. Jiménez, F. Garcia-Moreno, B. Pfretzschner, M. Klaus, M. Wollgarten, I. Zizak, G. Schumacher, M. Tovar, J. Banhart, Acta Mater 59, 6318 (2011).

[16]   J. Baumeister, German Patent DE40 18 360, 1990.

[17]   F. von Zeppelin, M. Hirscher, H. Stanzick and J. Banhart, Compos. Sci. Technol 63, 2293(2003).

[18]   Ch. Genzel, I. Denks, J. Gibmeier, M. Klaus, G. Wagener. Nucl Instr and Meth in Phys Res A 578, 23 (2007).

[19]   V. Raghavan, Journal of Phase Equilibria and Diffusion Vol. 26 No. 6 (2005).